Calculation of the reflectivity spectra dependence on the angle of incidence in anisotropic absorbing crystals, application to sodium nitrite

1990 J. Phys.: Condens. Matter 2 8791

(http://iopscience.iop.org/0953-8984/2/44/008)

J. Phys.: Condens. Matter 2 (1990) 8791–8800. Printed in the UK

Calculation of the reflectivity spectra dependence on the angle of incidence in anisotropic absorbing crystals, application to sodium nitrite

B Wyncke, F Bréhat and H Kharoubi

Laboratoire de Minéralogie, Cristallographie et Physique Infrarouge, URA 809 CNRS, Université de Nancy I, BP 239, 54506 Vandoeuvre lès Nancy Cédex, France

Received 18 December 1989, in final form 10 July 1990

Abstract. Explicit relations are given which allow the calculation of the infrared reflectivity spectra dependence on the angle of incidence for both polarizations in anisotropic absorbing crystals of symmetry as high or higher than orthorhombic. As an example, these relations are applied to the case of orthorhombic sodium nitrite. The calculated and experimental results are compared.

1. Introduction

Infrared reflectivity spectroscopy uses near normal incidence ($\leqslant 10°$) on plane plates cut parallel to the principal planes of the crystal, together with linear polarization of the incident electric field perpendicular to the plane of incidence, in order to observe the 'pure' reflectivity spectra and to avoid additional structures due to the influence of the angle of incidence or of the direction of polarization (Duarte *et al* 1987). In this case, polar phonons propagate along the principal crystal axes. When non-normal incidence together with linear polarization of the electric field in the plane of incidence are used in infrared reflectivity or transmission spectroscopy, reflection bands (Barker and Ilegems 1973, Goullet *et al* 1989) or absorption bands (Berreman 1963) are observed at frequencies characteristic of longitudinal optic modes.

Infrared reflectivity spectroscopy allows quantitative studies of anisotropic crystals in spectral regions corresponding to strong resonances of the crystal, where it becomes practically opaque, even for the thinnest obtainable samples. This technique is successfully used in the determination of the intrinsic optical constants of absorbing crystals, specifically the real and imaginary part of the complex refractive index: $\bar{n} = n + ik$. From the measurement of the infrared reflectivity spectrum $R(\omega)$ in a wide range of frequencies, the optical constants can be deduced by a fit of an appropriate dielectric function model to the experimental spectrum (Gervais 1983). To describe media which are absorbing, the conductivity is included as the imaginary part of the complex dielectric function (Born and Wolf 1959 section 14.6): $\bar{\varepsilon}_{ij}(\omega) = \varepsilon'_{ij}(\omega) + i\,\varepsilon''_{ij}(\omega)$. The real ε' and imaginary ε'' part of $\bar{\varepsilon}$ are symmetrical tensors, whose principal axes coincide only for symmetry classes as high or higher than orthorhombic (Born and Wolf 1959 section 14.6), they form the principal dielectric axes system (x, y, z), in which the symmetrical

0953-8984/90/448791 + 10 $03.50

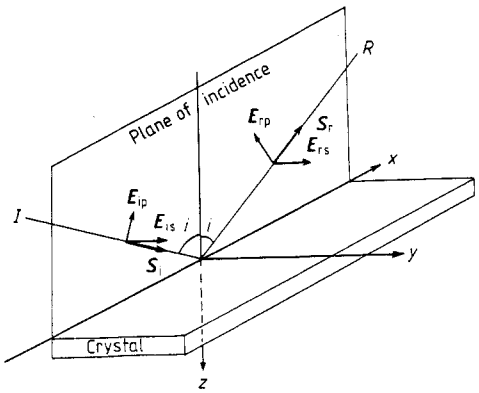

Figure 1. Principal axes of an anisotropic crystal x, y and z. The incident (I) and reflected (R) beams lie in the plane of incidence x–z. The two polarizations of the incident and reflected waves parallel (p) and perpendicular (s) to the plane of incidence are shown.

tensors ε'_{ij} and ε''_{ij} can both be diagonalized into their principal values. The principal values of the complex refractive index along these axes are related to the principal values of the complex dielectric function through the relation: $\bar{n}_k^2 = \bar{\varepsilon}_k$ $(k = x, y, z)$.

The aim of the present paper is to propose a way of calculating the infrared reflectivity spectra of absorbing crystals belonging to symmetry classes as high or higher than orthorhombic, in order to study their angular dependencies, for both polarizations parallel and perpendicular to the plane of incidence which coincide with a principal crystallographic plane. In section 2 we shall set out the expressions of the reflectivity of a plane interface between air and an absorbing orthorhombic crystal. As an example, the influence of the angle of incidence on the infrared reflectivity spectra of sodium nitrite will be calculated and compared to experimental results in section 3. $NaNO_2$ is chosen as an example because it has an orthorhombic structure, and five infrared active weakly damped lattice modes at 7 K, between 150 and 250 cm^{-1} (Bréhat and Wyncke 1985).

2. Reflectivity of a principal plane at oblique incidence

2.1. Boundary conditions

Let us consider two semi-infinite media separated by a plane interface, air or vacuum, and a non-magnetic, homogeneous orthorhombic absorbing crystal, containing no free charges or currents. In an infrared reflectivity experiment, a monochromatic electromagnetic plane wave of angular frequency ω incident in vacuum on the principal crystal x–y plane, gives rise to a reflected and a refracted wave at this plane. The electric field of the incident wave is linearly polarized whether parallel (p-polarization) or perpendicularly (s-polarization) to the plane of incidence which coincide with the principal x–z plane (figure 1). With these experimental conditions, it is well known from crystal optics that there exists only one reflected and one refracted wave, whose polarization is that of the incident wave, which propagate in the plane of incidence x–z (Bouasse 1925, Szivessy 1928) (figure 1).

The equations for calculating the reflectivity of anisotropic absorbing crystals were first formulated by Drude (1887), one century ago. We will derive them from the boundary conditions, namely the continuity of the tangential components of the electric $\boldsymbol{E}$ and magnetic $\boldsymbol{H}$ field of the incident (i), reflected (r) and refracted (t) wave, on the

interface between the two media (Born and Wolf 1959, section 1.1). Since for a plane wave $\boldsymbol{E}$ and $\boldsymbol{H}$ are in space quadrature, the $\boldsymbol{H}$ vector of an s-polarized wave lies in the plane of incidence (p-polarization), while for a p-polarized wave, the $\boldsymbol{H}$ vector is perpendicular to this plane (s-polarization). Thus, if z is the unit vector of the z axis, which is the normal to the crystal interface x–y (figure 1), the boundary conditions are written for s-polarization:

$$z \times \boldsymbol{E}_{is} + z \times \boldsymbol{E}_{rs} = z \times \boldsymbol{E}_{ts} \qquad z \times \boldsymbol{H}_{ip} + z \times \boldsymbol{H}_{rp} = z \times \boldsymbol{H}_{tp} \tag{1}$$

and for p-polarization:

$$z \times \boldsymbol{E}_{ip} + z \times \boldsymbol{E}_{rp} = z \times \boldsymbol{E}_{tp} \qquad z \times \boldsymbol{H}_{is} + z \times \boldsymbol{H}_{rs} = z \times \boldsymbol{H}_{ts}. \tag{2}$$

2.2. *Propagation of the refracted wave in the principal x–z plane of the absorbing crystal*

Let $\boldsymbol{s}_t$ be the unit vector of the direction of refraction of the monochromatic wave in the x–z plane of the absorbing crystal, and $\bar{n}$ the complex refractive index in this direction. Morsteller and Wooten (1968) have defined the complex wave-vector surface and the complex ray-vector surface, corresponding to such a wave, together with the dual relationship between these two complex surfaces. For each wave-normal vector direction, these two surfaces give respectively the values of the two complex refractive indices and those of the two complex magnitudes of the complex ray vector $\bar{\tau}\boldsymbol{t}_t$, associated with the wave-normal direction. $\boldsymbol{t}_t$ is the unit vector of the direction of the refracted ray. When the wave-normal vector $\bar{n}\boldsymbol{s}_t$ lies in any one of the three principal planes of an orthorhombic crystal determined by the principal dielectric axes, the two corresponding rays also lie in this plane (Born 1933 section 62). Thus for the refracted wave which propagates in the x–z plane, there are two values of the complex refractive index:

$$\bar{n}_1 = \bar{n}_y \tag{3}$$

$$\bar{n}_2^2 = \bar{n}_x^2 \bar{n}_z^2 / (\bar{n}_x^2 s_{tx}^2 + \bar{n}_z^2 s_{tz}^2) \tag{4}$$

and two complex magnitudes of the complex ray vector:

$$\bar{\tau}_1 = 1/\bar{n}_y \tag{5}$$

$$1/\bar{\tau}_2^2 = \bar{n}_z^2 t_{tx}^2 + \bar{n}_x^2 t_{tz}^2 \tag{6}$$

corresponding to the two principal waves $\boldsymbol{D}_1$ and $\boldsymbol{D}_2$ which can propagate in a given direction of the principal x–z plane. The former, defined by (1) and (3), is polarized perpendicularly to the x–z plane, the wave-normal vector coincides with the ray vector as the two $\boldsymbol{D}_1$ and $\boldsymbol{E}_1$ vectors, while the latter, defined by (4) and (6), is polarized linearly in the x–z plane. In general, though, the wave-normal vector does not coincide with the ray vector (Morsteller and Wooten 1968, Piro 1987). However, the magnetic and electric fields of these two waves are always in space quadrature, and related by

$$\boldsymbol{H}_j = \sqrt{(\varepsilon_0/\mu_0)}\bar{n}_j \boldsymbol{s}_t \times \boldsymbol{E}_j \tag{7}$$

where $j = 1$ for s-polarization and $j = 2$ for p-polarization.

2.3. *Reflectivity at oblique incidence*

Let us now consider the energy flow in air or vacuum ($\bar{n} = 1$) in which the incident and reflected wave propagate, the refracted wave being completely absorbed in the crystal.

Following Born and Wolf (1959 section 1.5.3) the reflectivity of the crystal plane interface is defined by the ratio of the amount of the energy leaving the unit area of the interface per second to the amount of energy which is incident per second on this unit area. For a polarized wave this gives (Salzberg 1948)

$$R_v = \bar{r}_v \bar{r}_v^* = |\bar{r}_v|^2 \qquad (v = p, s)$$

where $\bar{r}$ is the complex electric amplitude reflection and magnetic amplitude reflection coefficient: $\bar{r} = E_r/E_i = H_r/H_i$ (Salzberg 1948), and * indicates the complex conjugate. Thus the reflectivity for an s-polarized wave is defined by the ratio:

$$R_s = |E_{rs}/E_{is}|^2 = |H_{rp}/H_{ip}|^2 \tag{8}$$

$$R_p = |H_{rs}/H_{is}|^2 = |E_{rp}/E_{ip}|^2 \tag{9}$$

is the reflectivity for a p-polarized wave.

2.3.1. Reflectivity for an s-polarized wave. Let E_{is}, E_{rs}, E_{ts} and H_{ip}, H_{rp}, H_{tp} be the amplitudes of the electric and magnetic fields of the incident, reflected and refracted wave. Using the boundary conditions (1) and relation (7) with $j = 1$ for the refracted wave, $\bar{n}_j \boldsymbol{s}_t = \boldsymbol{s}_i$ for the incident and $\bar{n}_j \boldsymbol{s}_t = \boldsymbol{s}_r$ for the reflected waves in the vacuum ($\bar{n}_j = 1$), ($\boldsymbol{s}_i$ and $\boldsymbol{s}_r$ are the unit vectors of the direction of the incident and reflected wave), a straightforward calculation gives the relations:

$$E_{is} + E_{rs} = E_{ts} \qquad (E_{is} + E_{rs}) s_{iz} = E_{ts} \bar{n}_y s_{tz} \tag{10}$$

where $s_{iz} = \cos i$ and $s_{tz} = \cos t$, i and t are respectively the angle of incidence and the angle of refraction, related through the complex Snell's law: $\sin i = \bar{n}_y \sin t$, where $\sin t$ is a complex quantity. From (10) we deduce

$$\bar{r}_s = E_{rs}/E_{is} = [\cos i - (\bar{n}_y^2 - \sin^2 i)^{1/2}]/[\cos i + (\bar{n}_y^2 - \sin^2 i)^{1/2}]. \tag{11}$$

The complex quantity $(\bar{n}_y^2 - \sin^2 i)^{1/2}$ which appears in (11) can be related to the optical constants of the crystal n_y and k_y, the refractive index and index of absorption along the y axis, if we set

$$(\bar{n}_y^2 - \sin^2 i)^{1/2} = \bar{n}_y \cos t = a_y + \mathrm{i}\, b_y \tag{12}$$

where a_y and b_y are real quantities related to the optical constants and to the angle of incidence through the relations:

$$a_y = [\![\tfrac{1}{2}\{[(n_y^2 - k_y^2 - \sin^2 i)^2 + 4n_y^2 k_y^2]^{1/2} + (n_y^2 - k_y^2 - \sin^2 i)\}]\!]^{1/2} \tag{13a}$$

$$b_y = [\![\tfrac{1}{2}\{[(n_y^2 - k_y^2 - \sin^2 i)^2 + 4n_y^2 k_y^2]^{1/2} - (n_y^2 - k_y^2 - \sin^2 i)\}]\!]^{1/2} \tag{13b}$$

Thus from (8) and (11) we obtain the explicit expression for the reflectivity R_s, in terms of the optical constants and of the angle of incidence given by relations (13)

$$R_s = [(\cos i - a_y)^2 + b_y^2]/[(\cos i + a_y)^2 + b_y^2] \tag{14}$$

2.3.2. Reflectivity for a p-polarized wave. The two binary systems of equations (1) and (2) are similar, they differ only by the polarization of the $\boldsymbol{E}$ and $\boldsymbol{H}$ vectors. Using the duality rule between the complex wave-vector and ray-vector surfaces (Morsteller and Wooten 1968) i.e. by replacing the electric field amplitudes by the magnetic ones for the

same polarization, and the complex wave vector $\bar{n}s$ by the complex ray vector $\bar{\tau}t$, the boundary conditions (2) are written from (10) in the form

$$(H_{is} - H_{rs})t_{iz} = H_{ts}\bar{\tau}_2 t_{tz} \qquad H_{is} + H_{rs} = H_{ts} \tag{15}$$

where in the vacuum $t_{iz} = s_{iz} = \cos i$ and in the absorbing crystal we obtain from (6): $\bar{\tau}_2 t_{tz} = (\bar{n}_z^2 - \sin^2 i)^{1/2}/\bar{n}_x\bar{n}_z$. From (15) we deduce

$$\bar{r}_p = H_{rs}/H_{is} = [\bar{n}_x\bar{n}_z \cos i - (\bar{n}_z^2 - \sin^2 i)^{1/2}]/[\bar{n}_x\bar{n}_z \cos i + (\bar{n}_z^2 - \sin^2 i)^{1/2}]. \tag{16}$$

It is useful to set: $\bar{n}_x\bar{n}_z = A + iB$, to express the product in terms of the optical constants of the crystal, according to the relations:

$$A = n_x n_z - k_x k_z \quad \text{and} \quad B = n_x k_z + n_z k_x \tag{17}$$

and once again $(\bar{n}_z^2 - \sin^2 i)^{1/2} = \bar{n}_z \cos t = a_z + ib_z$, where a_z and b_z are given by relations (13). Thus from (9) and (16) we obtain the explicit relation for the reflectivity R_p, in terms of the optical constants and of the angle of incidence given by relations (17) and (13)

$$R_p = [(A \cos i - a_z)^2 + (B \cos i - b_z)^2]/[(A \cos i + a_z)^2 + (B \cos i + b_z)^2]. \tag{18}$$

Relations (14) and (18) evaluated for propagation in the principal x–z plane, are valid for propagation in the two other principal planes x–z and y–z of the orthorhombic class, thus all six permutations of the cartesian indices are valid in (14) and (18). These relations are also valid for uniaxial symmetry classes, if the complex refractive indices $\bar{n}_x$ and $\bar{n}_y$ are replaced by the complex ordinary refractive index $\bar{n}_0$, and $\bar{n}_z$ by the complex extraordinary index $\bar{n}_e$.

If we consider normal incidence, equations (14) and (18) reduce to the well known relation

$$R_l = |(\bar{\varepsilon}_l^{1/2} - 1)/(\bar{\varepsilon}_l^{1/2} + 1)|^2 = [(1 - n_l)^2 + k_l^2]/[(1 + n_l)^2 + k_l^2] \qquad (l = x, y, z) \tag{19}$$

3. Influence of the angle of incidence on the infrared reflectivity spectra of sodium nitrite

3.1. Infrared reflectivity spectra of $NaNO_2$

Sodium nitrite is orthorhombic in its low temperature ferroelectric phase, with space group symmetry C_{2v}^{20}(Im2m) and one formula unit in the primitive cell. Group theory allows five infrared lattice modes:

$$2B_2(E\|a) + 1A_1(E\|b) + 2B_1(E\|c).$$

The polarization direction of each lattice mode is indicated in the brackets a, b and c refer to the designation of the biaxial axes (Bréhat and Wyncke 1985).

We have studied the infrared reflectivity spectra polarized along the three crystallographic axes of $NaNO_2$, from 5 to 600 cm^{-1}, in the temperature range 7–500 K, and determined the lattice mode parameters of the five infrared active lattice modes together with the parameters of the low frequency excitations of relaxation type, which explain the submillimetre dielectric response (Wyncke *et al* 1984, Kozlov *et al* 1985, Bréhat and

Table 1. Lattice mode parameters of $NaNO_2$ at 7 K: frequencies Ω_j and damping γ_j in cm^{-1}. Damping factors γ_L^R, γ_T^R are expressed in cm^{-1}. Strength S_{Dj} and relaxation time τ_j (in cm) characterize the Debye relaxation model for A_1 symmetry species (see text).

	J	Ω_{TO}	Ω_{LO}	γ_{TO}	γ_{LO}	S_{Dj}	τ_j
A_1	1	200	280	4	13	1.5	7.5
						0.2	0.02
		Ω_{TO}	Ω_{LO}	γ_{TO}	γ_{LO}	γ_L^R	γ_T^R
B_1	1	163.5	175.7	1.5	1.5	195	183
	2	202.5	264.5	4	12		
B_2	1	156	204.5	4.5	2	70	67
	2	237.5	277.5	5	16		

Wyncke 1985). The lattice mode parameters and the relaxation parameters at 7 K are reported in table 1.

Two models have been used for the simulation of the $NaNO_2$ reflectivity spectra:

(i) for B_1 and B_2 symmetry species, we used relation (19) and the factorized form of the dielectric function

$$\bar{\varepsilon}(\omega) = \varepsilon_\infty \frac{\omega - i\gamma_L^R}{\omega - i\gamma_T^R} \prod_j \frac{\Omega_{jLO}^2 - \omega^2 + i\omega\gamma_{jLO}}{\Omega_{jTO}^2 - \omega^2 + i\omega\gamma_{jTO}} \tag{20}$$

where the relaxation is characterized by the damping factors γ_L^R and γ_T^R, Ω_j and γ_j represent the frequencies and dampings of the transverse (TO) and longitudinal (LO) optical modes, and ε_∞ is the high frequency dielectric constant (Wyncke *et al* 1984, Bréhat and Wyncke 1985).

(ii) for A_1 symmetry, we used relation (19) and the dielectric function

$$\bar{\varepsilon}(\omega) = S_{D1}/(1 + i\omega\tau_1) + S_{D2}/(1 + i\omega\tau_2) + \varepsilon_\infty(\Omega_{LO}^2 - \omega^2 + i\omega\gamma_{LO})/\Omega_{TO}^2 - \omega^2 + i\omega\gamma_{TO}) \tag{21}$$

where we consider three contributions: one A_1 lattice mode and two Debye relaxations, S_{Dj} and τ_j being respectively the strength and the relaxation time (Kozlov *et al* 1985, Bréhat and Wyncke 1985). The imaginary part $\varepsilon''(\omega)$ is always positive in the spectral range 0–600 cm^{-1} when the parameters of table 1 are used with relations (20) and (21).

Equation (20) and the corresponding parameters of table 1 are used to calculate the optical constants n and k, along the a and c axis, relation (21) and the corresponding parameters of table 1 are used for those along the b axis. These optical constants will be used in the next section to calculate the $NaNO_2$ infrared reflectivity spectra at oblique incidence.

3.2. Infrared reflectivity spectra of $NaNO_2$ at oblique incidence

3.2.1. Experimental study. We have studied the infrared reflectivity spectra along the three crystallographic axes of $NaNO_2$ (s-polarization) with an angle of incidence of 30°,

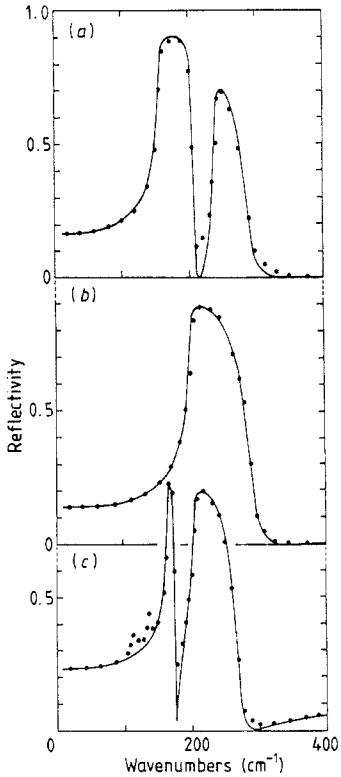

Figure 2. Infrared reflectivity spectra of $NaNO_2$, polarized along the three crystallographic axes at 7 K: (*a*) $\boldsymbol{E} \| a$, (*b*) $\boldsymbol{E} \| b$ and (*c*) $\boldsymbol{E} \| c$. The incident s-polarized wave makes an angle of 30° with the normal to the plane plate. Full curves correspond to the calculated reflectivity spectra using equations (14) and (13) (see text). Dots represent experimental measurements.

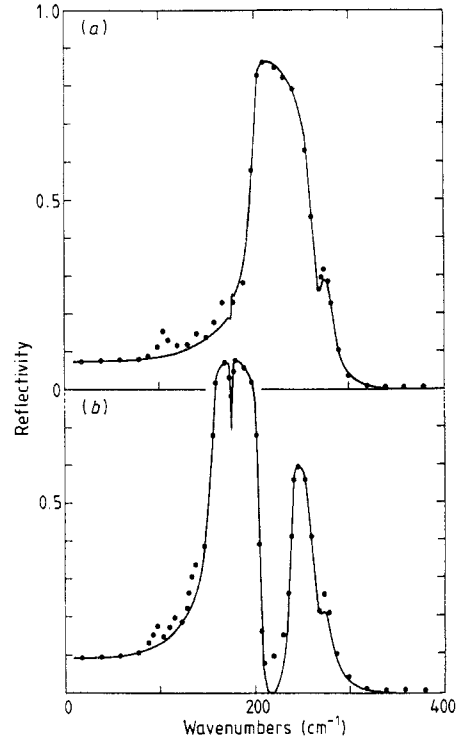

Figure 3. Infrared reflectivity spectra of a $NaNO_2$ *a–b* plane plate at 7 K. (*a*) the incident p-polarized wave propagates in the *b–c* principal plane at an angle of 30° from the *c* axis. (*b*) the incident p-polarized wave propagates in the *a–c* principal plane at an angle of 30° from the *c* axis. Full curves correspond to the calculated reflectivity spectra using equations (18), (17) and (13) (see text). Dots represent experimental measurements.

Table 2. Symmetry and character of the infrared excited modes for p-polarization.

Interface	*a–b*		*b–c*		*a–c*	
Plane of incidence	*b–c*	*a–c*	*a–c*	*a–b*	*a–b*	*b–c*
Pure TO and LO modes: $i = 0°$	A_1	B_2	B_1	A_1	B_2	B_1
LO modes excited $i > 20°$	B_1	B_1	B_2	B_2	A_1	A_1

at 7 K between 15 and 400 cm^{-1}. Figure 2 displays the experimental results which are in agreement with our previous study for the *a* and *b* axes (Bréhat and Wyncke 1985), whereas two weak structures are observed at 139 and 115 cm^{-1} along the *c* axis, in addition to the two B_1 infrared lattice modes (table 1).

The infrared reflectivity spectra for the six possible cases of p-polarization for orthorhombic $NaNO_2$ (table 2), were carefully studied between 15 and 400 cm^{-1} at 7 and

300 K, for incidence angles 10 and 30°. Figure 3 displays the more significant experimental results for the reflectivity of the *a–b* principal plane at 7 K, the electric field being linearly polarized in the *b–c* and in the *a–c* principal plane. As for s-polarized B_1 spectrum (figure 2), several weak structures are observed below 150 cm^{-1}, at 139, 115 and 100 cm^{-1} (figure 3).

3.2.2. Calculated reflectivity spectra

3.2.2.1. s-polarization. The infrared reflectivity spectra polarized along the three principal axes of $NaNO_2$ were calculated at 7 K, for the angle of incidence i varying from 0 to 90°, using relations (14) and (13) and the corresponding optical constants calculated as explained in section 3.1. Figure 2 displays the agreement between the calculated and the experimental reflectivity spectrum for $i = 30°$. It is to be noted that the difference between the reflectivity spectra for $i = 0°$ and $i = 10°$ is negligible, and this justifies the use of an angle of incidence $\leqslant 10°$ in many infrared reflectivity experiments.

3.2.2.2. p-polarization. The infrared reflectivity spectra for the six possible cases of p-polarization for orthorhombic $NaNO_2$ (table 2), were calculated at 7 K for the angle of incidence i varying from 0 to 90°, using relations (18), (17) and (13) and the corresponding optical constants calculated as explained in section 3.1. Figure 3 displays the agreement between the calculated and the experimental reflectivity spectra of a $NaNO_2$ *a–b* principal plane at 7 K for $i = 30°$.

Off-normal incidence effects manifest themselves only when $i \geqslant 20°$ for p-polarization. For a finite value of the angle of incidence, the p-polarized incident waves have two electric field components E_x and E_z (figure 1), such that they first couple through E_x to the TO modes of the symmetry species corresponding to the x axis and second, through E_z, to the LO modes of symmetry species corresponding to the z axis. This results in a strong energy loss when the frequency of the incident wave equals a LO mode frequency. Three cases are to be considered according to the relative position of the $(LO)_z$ frequency with respect to the frequency range $(TO)_x$–$(LO)_x$ of the x symmetry species:

(i) when a $(LO)_z$ frequency is located between two $(TO)_x$–$(LO)_x$ modes, for low values of the angle of incidence, a small dip appears around the $(LO)_z$ frequency, which becomes stronger with the increase in the angle of incidence, and keeps a constant frequency value in the case of weak mode damping.

(ii) when a $(LO)_z$ frequency is located on the high-frequency side, outside the frequency range $(TO)_x$–$(LO)_x$, and falls in a region of low reflectivity, in this case a narrow 'spikelike' structure is predicted by the calculation.

(iii) when a $(LO)_z$ frequency again falls outside the $(TO)_x$–$(LO)_x$ frequency range, but on the low-frequency side, the calculated reflectivity spectrum displays a more complex structure.

The three behaviours predicted by the calculation are observed in the experimental infrared reflectivity spectra of $NaNO_2$ for p-polarization (figure 3), due to the relative position of the TO and LO mode frequencies and to the weak damping of the infrared active lattice modes at 7 K (table 1). As an example, figure 3 displays the three possible off-normal incidence effects for the principal *a–b* plane: in figure 3(*a*), the dip at 270 cm^{-1} is due to the excitation of the B_1 LO_2 mode frequency, case (i), and the structure at 175 cm^{-1} to the B_1 LO_1 mode frequency, case (iii); in figure 3(*b*), the dip at 175 cm^{-1} is due to the excitation of the B_1 LO_1 mode frequency, case (i), and the spike at 275 cm^{-1} to the

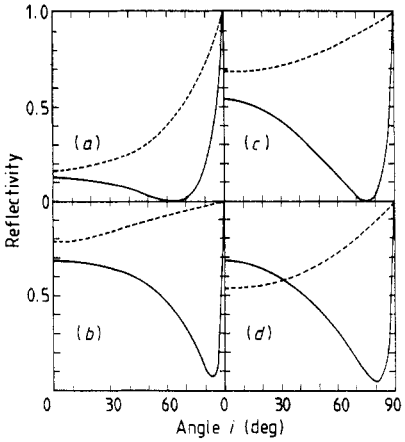

Figure 4. Calculated reflectivity of $NaNO_2$ at 7 K. $R_s(i)$ (equation 14) (broken curves) and $R_p(i)$ (equation 18) (full curves), versus angle of incidence i, at a fixed frequency ω. (a) ω = 100 cm^{-1}, the incident s wave is polarized along the a axis, and the p incident wave in the b–c principal plane. (b) ω = 200 cm^{-1}, polarization as in (a). (c) ω = 200 cm^{-1}, the incident s-wave is polarized along the b axis, and the p-incident wave in the a–c principal plane. (d) ω = 200 cm^{-1}, the incident s-wave is polarized along the c axis, and the p-incident wave in the a–b principal plane.

B_1 LO_2 mode frequency, case (ii). At 300 K the mode dampings are increased by a factor of at least 5 (Bréhat and Wyncke 1985), the off-normal incidence effects disappear completely in the calculated and experimental reflectivity spectra, together with the additional weak structures observed below 150 cm^{-1} at 7 K.

3.2.3. Variation of the reflectivity with the angle of incidence at a fixed frequency. The reflectivity of an s- or p-polarized monochromatic plane wave, incident in vacuum on a principal plane of an absorbing anisotropic crystal, is governed respectively by relation (14) or (18), and depends on the angle of incidence i. The behaviour of the functions $R_s(i)$ (14) and $R_p(i)$ (18) at fixed frequencies is calculated for $NaNO_2$ at 7 K in the infrared frequency range, where the dielectric function $\bar{\varepsilon}$ is complex.

As the angle of incidence increases from 0 to 90°, $R_s(i)$ increases monotonically from a minimum at normal incidence (i = 0°) to 1 at grazing incidence (i = 90°) (figure 4). On the other hand, $R_p(i)$ first decreases to a minimum and then increases to 1 at grazing incidence (figure 4). Complete extinction of the p-polarized reflected wave is observed below 150 cm^{-1} at the Brewster angle, for the six possible orientations studied in orthorhombic sodium nitrite, due to the very low values of the index of absorption in this frequency range. For ω = 100 cm^{-1} (figure 4(a)), the Brewster angle is 63°, and the index of absorption is about 0.03, whereas the minimum of the reflectivity $R_p(i)$ is always non-zero above 150 cm^{-1} at the so-called pseudo-Brewster angle, as shown for 200 cm^{-1} by figures 4(b), 4(c) and 4(d), on which the pseudo-Brewster angles are respectively 84°, 75° and 80°. This frequency range corresponds to the dispersion region of $NaNO_2$ in which the index of absorption is higher than 1.

4. Discussion

In the present paper, using sodium nitrite as an example, we have shown that the expressions of the reflectivity (14) and (18), worked out in section 2, allow the calculation

of the infrared reflectivity spectra dependence on the polarization of the incident wave and on the angle of incidence. Such calculations could provide an explanation for extra features observed in the experimental reflectivity spectra or differences between the experimental reflectivity spectra published by different authors that are caused by the finite angle of incidence of the light beam. This angle could be as high as 20° in most cases due to the convergency of the light beams in spectrometers.

The effect of the finite incidence angle on the polarized infrared reflectivity spectra of $NaNO_2$ has been investigated in great detail at 7 K. The experimental results are compared to the calculated reflectivity spectra obtained by using relations (14) and (18), and are in good agreement as shown by figures 2 and 3 for an angle of incidence of 30°. $NaNO_2$ is a good example to illustrate such a study because of its orthorhombic structure and its five infrared active lattice modes whose parameters are known (table 1). Such calculations can also be done for any anisotropic absorbing crystal of symmetry as high as or higher than orthorhombic.

Off-normal incidence effects appear only for p-polarized waves in the frequency range of the lattice modes, i.e. 150–300 cm^{-1} in the case of $NaNO_2$ (figure 3), and are strongly dependent on the angle of incidence. It is to be noted that the low-frequency excitations of relaxational character active in $NaNO_2$, (table 1), did not manifest themselves in the off-normal calculated reflectivity spectra (figures 2 and 3).

In the case of $NaNO_2$, off-normal incidence effects cannot be the cause of the additional structures observed below 150 cm^{-1} in the s-polarized $E\|c$ spectrum (figure 2) or in the p-polarized spectra (figure 3), that have been reported in the present work for the first time. These weak modes observed only at 7 K can be related to the activity of disorder induced modes or Raman active modes at low temperature. The study of $NaNO_2$ Raman spectra at 10 K has shown the activity of an A_2 mode at 139 cm^{-1} (Kugel 1990) and this is the frequency of one of the observed weak modes at 7 K (figures 2 and 3).

References

Barker A S and Ilegems M 1973 *Phys. Rev.* B **7** 743
Berreman D W 1963 *Phys. Rev.* **130** 2193
Born M 1933 *Optik* (Berlin: Springer)
Born M and Wolf E 1959 *Principles of Optics* (Oxford: Pergamon)
Bouasse H 1925 *Propagation de la Lumière* (Paris: Delagrave) ch 6
Bréhat F and Wyncke B 1985 *J. Phys. C: Solid State Phys.* **18** 1705
Drude P 1887 *Ann. Phys., Lpz.* **32** 584
Duarte J L, Sanjurjo J A and Katiyar R S 1987 *Phys. Rev.* B **36** 3368
Gervais F 1983 *Infrared and Millimeter Waves* vol 8, ed K J Button (New York: Academic) ch 7
Goullet A, Camassel J, Martin L, Pascual J and Philippot E 1989 *Phys. Rev.* B **40** 5750
Kozlov G V, Kryukova E B, Wyncke B, Bréhat F and El Sherif M 1985 *Phys. Status Solidi* b **127** 465
Kugel G 1990 private communication
Morsteller L P and Wooten F 1968 *J. Opt. Soc. Am.* **58** 511
Piro O E 1987 *Phys. Rev.* B **36** 3427
Salzberg B 1948 *Am. J. Phys.* **16** 444
Szivessy G 1928 *Handbuch der Physik* vol 20 (Berlin: Springer) p 715
Wyncke B, Bréhat F, El Sherif M and Kozlov G V 1984 *Phys. Status Solidi* b **125** 493